Spiers Memorial Lecture

Recent experimental advances in studies of liquid/liquid interfaces

Megan A. Leich and Geraldine L. Richmond

Department of Chemistry, University of Oregon, Eugene OR 97403-1253, USA

Received 11th October 2004, Accepted 11th October 2004
First published as an Advance Article on the web 22nd November 2004

Liquid/liquid interfaces play a key role in many important processes. Studying the molecular structure and interactions that occur at these interfaces can aid in our understanding of more complicated processes such as molecular transport across cell membranes. A variety of techniques have been applied to this pursuit. Here we present selected examples of exciting recent studies using different techniques to examine liquid/liquid interfaces.

Introduction

Liquid surfaces and interfaces have a central part in many chemical, physical, and biological processes. Many important processes occur at the interface between water and a hydrophobic liquid. Separation techniques are possible due to the hydrophobic/hydrophilic properties of liquid/liquid interfaces. In biological systems, protein folding and membrane formation rely on the interaction of a hydrophobic surface with water, and ion and solute transport across these and other liquid/liquid interfaces are dependent on the interaction between the interfacial molecules in the hydrophobic fluid and the hydrophilic fluid with the ion or solute being studied. Reactions that proceed at interfaces are also highly dependent on the interactions between the interfacial solvent and solute molecules.

The interfacial structure and properties of molecules at these interfaces are generally very different from those in the bulk. Therefore, an understanding of the chemical and physical properties of these systems is dependent on an understanding of the interfacial molecular structure. However, these properties have traditionally been difficult to study at liquid/liquid interfaces, due to the buried nature of the system. For example, most spectroscopic techniques analyze the molecules in the bulk as well as those at the interface. Since there are considerably more bulk molecules than interfacial molecules, the spectral features arising from molecules at the interface are often overwhelmed by those from the bulk molecules. It is therefore necessary to use a surface-sensitive technique to study these interfacial molecules.

Recent developments in experimental surface techniques have facilitated the study of liquid/liquid interfaces. Some of these methods specifically probe interfacial molecules, while others are traditionally bulk techniques that have been adapted to study the interface. Second-harmonic generation and vibrational sum-frequency spectroscopy both provide molecular information that is inherently surface-specific. Ellipsometry and Brewster angle microscopy are also interfacial techniques. Ellipsometry has been used to provide information about adsorption and changes in

molecular orientation at interfaces, while Brewster angle microscopy has recently been adapted to yield images of the adsorbate domain formation at liquid/liquid interfaces. Fluorescence spectroscopy has been used in several unique ways to provide insight into the environment of interfacial molecules. X-ray and neutron scattering have also recently been applied to liquid/liquid interfaces with impressive results. Here, we will present a few examples of recent applications of experimental techniques to the study of liquid/liquid interfaces. This is by no means meant to be a comprehensive review of the field. Instead, snapshots of recent progress in selected areas are provided, and more detailed information is available in the literature.

Surface second harmonic generation

Since the technique was pioneered more than twenty years ago, second harmonic generation (SHG) has proven to be a useful tool for studying interfacial molecular properties such as symmetry, orientation and number density of adsorbed molecules, and interfacial dielectric properties.[1–4] The first application of this technique to the study of liquid/liquid interfaces occurred in 1988.[5] Since then, a variety of liquid/liquid interfaces have been studied with SHG.[6,7]

Second harmonic generation is a second-order nonlinear spectroscopy and, under the electric dipole approximation, is forbidden in isotropic media, making it inherently surface-specific.[8] In SHG, a laser beam is directed onto an interface and generates another beam at twice the incident frequency. The intensity of the SHG beam is related to the resonant and the nonresonant contributions to the nonlinear susceptibility

$$I(2\omega) \propto |\chi_{\mathrm{NR}}^{(2)} + \chi_{\mathrm{Re},s}^{(2)}|^2 I^2(\omega) \tag{1}$$

where χ_{NR} and $\chi_{\mathrm{Re},s}$ are the nonresonant and resonant nonlinear susceptibility, respectively, and $I(\omega)$ is the intensity of the incident beam. The nonresonant contribution is generally much smaller than the resonant, which can be described by

$$\chi_{\mathrm{Re},s}^{(2)} = N \sum_{\mathrm{k,e}} \frac{\langle A_{\mathrm{k,e}} \rangle}{(\omega_{gk} - \omega - i\Gamma)(\omega_{\mathrm{eg}} - 2\omega + i\Gamma)} \tag{2}$$

where N is the number of probed molecules, ω_{ij} is the transition energy between the ground state and the states k and e, $\langle A_{\mathrm{k,e}} \rangle$ is the orientational average of the molecular hyperpolarizability, and Γ is the transition line width. When 2ω is resonant with ω_{eg}, $\chi_{\mathrm{Re},s}^{(2)}$ becomes large, enhancing the SHG intensity. By measuring the scaled intensity $I(2\omega)/I^2(\omega)$ as a function of 2ω, the excitation spectrum of a solute at an interface can be obtained. Since the effect relies on the resonant enhancement of $\chi_{\mathrm{Re},s}^{(2)}$, it is necessary to use a probe molecule that has a chromophore sensitive at an appropriate wavelength. Two selected examples of how SHG has been used to probe liquid/liquid interfaces are given below.

Knowledge of the changes in polarity at liquid/liquid interfaces is key to understanding the processes that occur at these interfaces. Polarity scales have helped to provide insight into processes in bulk solvents, but such a scale did not exist for liquid/liquid interfaces until recently. In 1998, Wang *et al.* developed an interfacial polarity scale based on their SHG measurements of the polarities of the water/chlorobenzene and water/1,2-dichloroethane interfaces.[9] Using the probe molecule *N*,*N*-diethyl-*p*-nitroaniline (DEPNA), shown in Fig. 1a, the positions of intramolecular π–π^* charge transfer (CT) absorption bands were measured for DEPNA at these interfaces and used as an indicator of the interfacial solvent polarity. In order to develop a polarity scale that is independent of the probe molecule, the polarity of the air/water interface was measured by both DEPNA and another probe molecule, 4-(2,4,6-triphenylpyridinium)-2,6-diphenylphenoxide ($E_T(30)$), shown in Fig. 1b. The bulk polarity scale of $E_T(30)$, known as the $E_T(30)$ scale, is well established, and is one of the most comprehensive polarity scales. From the measured excitation wavelengths for both probe molecules, similar polarities of the air/water interface were calculated, indicating that the measured value is a good representation of the polarity of the air/water interface.

The interfacial CT wavelengths were also compared with the transition wavelengths in bulk liquids (Fig. 2). From these results, it was determined that the interfacial polarity has a very simple relationship to the polarities of the two liquids forming the interface: the interfacial polarity is the

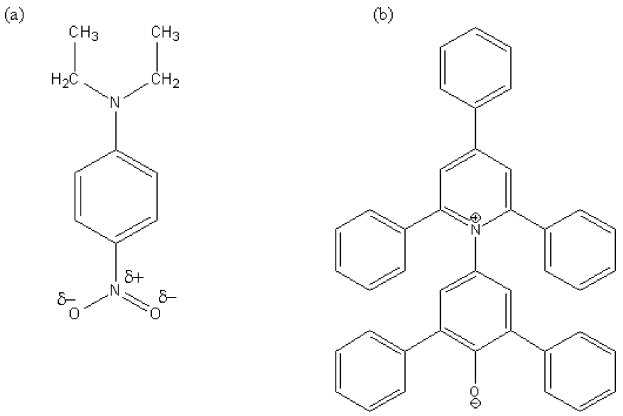

Fig. 1 (a) *N*,*N*-diethyl-*p*-nitroaniline (DEPNA). (b) 4-(2,4,6-Triphenylpyridinium)-2,6-diphenylphenoxide ($E_T(30)$).

average of the polarities of the two bulk phases

$$P_{A/B} = \frac{P_A + P_B}{2} \tag{3}$$

where $P_{A/B}$ is the polarity of the interface between liquids A and B, and P_A and P_B are the polarities of the bulk liquids. This relationship suggests that the difference in the ground and excited state interface solvation energies may be largely due to long-range, or solute–bulk solvent, interactions rather than local, or solute–interfacial solvent, interactions.

A second recent example of the application of SHG to liquid/liquid interfaces focuses on measuring the width of the interfacial region. Steel and Walker used a class of molecules known as ''molecular rulers'' to measure the width of liquid/liquid interfaces.[10] These molecules consist of a hydrophobic, solvatochromic probe based on *p*-nitroanisole with an anionic sulfate group attached by different length alkyl spacers (Fig. 3). At the liquid/liquid interface, the anionic sulfate group remained in the aqueous phase, while the hydrophobic spacer and chromophore extended into the organic phase. Using different length alkyl spacers allowed the distance the probe penetrated into the organic phase to be adjusted. By monitoring the excitation wavelength of the probe molecule as a function of chain length, they were able to determine the distance required to change the solvent polarity from the aqueous to the organic limit.

Fig. 4 shows SHG spectra of molecular rulers at the weakly associating cyclohexane/water interface. In bulk cyclohexane, the excitation maxima of the chromophores are centered around 295 ± 2 nm, and in bulk aqueous solution the maxima are at 318 ± 2 nm. When *p*-nitroanisole without an alkyl chain is adsorbed at the cyclohexane/water interface, the intensity maximum in the SHG spectrum occurs at 308 nm, which is consistent with the above assertion that interfacial polarity is the average of the polarities of the two bulk liquids.[9] As the chain length of the alkyl spacer increases from two to four to six carbons, the SHG maximum exhibits a shift towards the cyclohexane limit, indicating that the probe molecule is in an increasingly polar environment. Since the six-carbon chain molecular ruler samples a nonpolar environment, the interfacial environment changes from polar to nonpolar in less than 9 Å. These results suggest that the dipolar width, which is the distance for a dielectric environment to change from one phase to another, is molecularly sharp.

In contrast with the cyclohexane/water interface, the 1-octanol/water interface undergoes strong hydrogen bonding interactions between the two layers. Fig. 5 shows SHG spectra of the 1-octanol/water interface with C_2, C_4, C_6, and C_8 molecular rulers adsorbed to the interface. The window between the bulk excitation wavelengths for 1-octanol and water extends from 303 nm (bulk 1-octanol) to 318 nm (bulk water), but the SHG maximum for the adsorbed C_2 molecular rulers adsorbed at the 1-octanol/water interface is at 285 ± 2 nm, which is well outside the window. As the molecular ruler length is increased, the SHG maximum shifts to longer wavelengths. From these

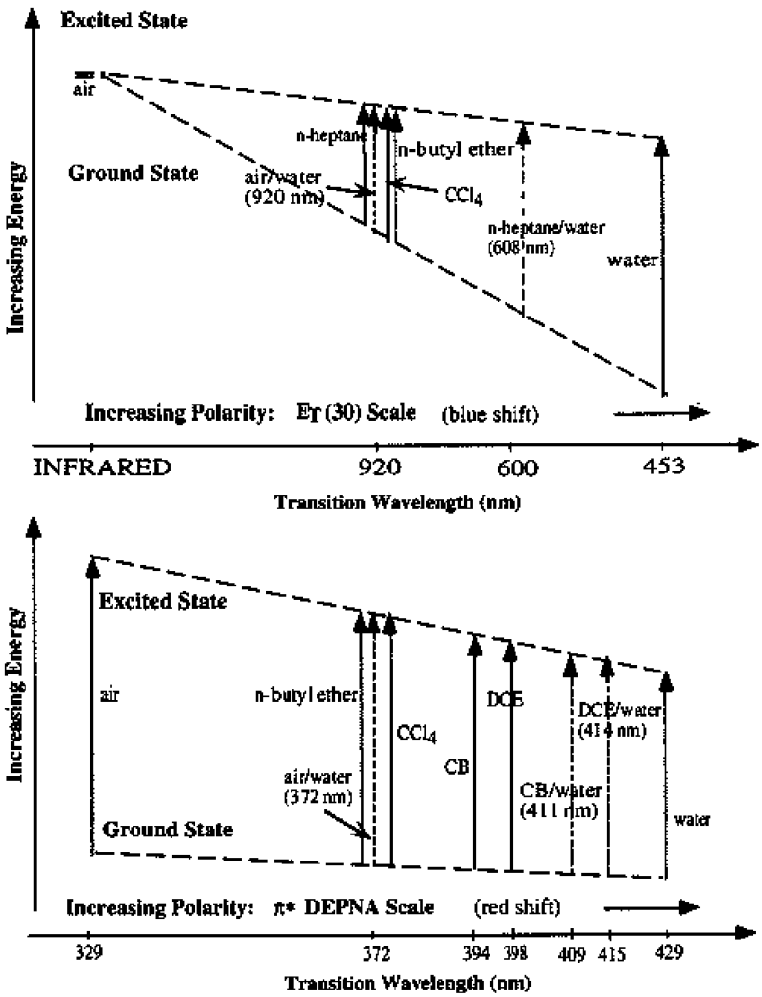

Fig. 2 $E_T(30)$ and DEPNA polarity scales. Observed transition wavelengths for $E_T(30)$ and DEPNA in bulk liquids and interfaces. CB is chlorobenzene and DCE is 1,2-dichloroethane. Solid arrows represent transitions in bulk liquids, and dotted arrows represent transitions at interfaces. The bracketed wavelengths are the predicted interface transition wavelengths. Reprinted with permission from ref. 9. © American Chemical Society 1998.

results, it was concluded that the adsorbed C_2 molecular ruler experienced an interfacial polarity that was less than that of either bulk phase. As the ruler length increased, the dielectric environment approached the polarity of the bulk solution. These spectra suggest that the 1-octanol undergoes surface-induced ordering, causing the interfacial octanol molecules to orient with the OH group toward the water layer and the eight-carbon chain pointing into the bulk octanol, creating a hydrophobic region between the polar layers of 1-octanol and water.

Vibrational sum-frequency spectroscopy

Vibrational sum-frequency spectroscopy (VSFS) is another second-order nonlinear optical method that is being increasingly applied to liquid/liquid interfaces. Like SHG, VSFS is inherently surface-specific. However, VSFS has the advantage over SHG of measuring the vibrational spectrum of the interfacial molecules. VSFS relies on the resonance between the infrared vibrational modes of the interfacial molecules and the tunable infrared beam for enhancements to the signal intensity. In

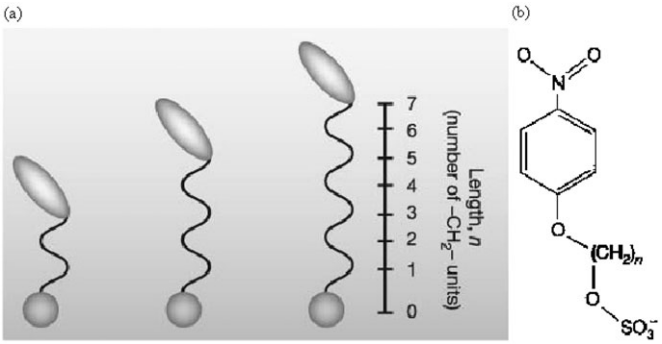

Fig. 3 Schematic representation of adsorbed molecular ruler surfactants, and their general structure. (a) Schematic representation of molecular ruler surfactants adsorbed to a liquid/liquid interface. As the alkyl spacer between the headgroup (circle) and solvatochromic chromophore (ellipse) lengthens, the hydrophobic probe can extend further into the organic phase. Correlating ruler length (in $–CH_2–$ units) with chromophore excitation wavelength enables experiments to determine the distance required for interfacial solvent polarity to converge to the organic limit. (b) General structure of molecular ruler surfactants. Surfactants are referred to as C_n rulers, where n corresponds to the number of methylene ($–CH_2–$) groups in the alkyl spacer. Reprinted with permission from ref. 10. © Nature Publishing Group 2003.

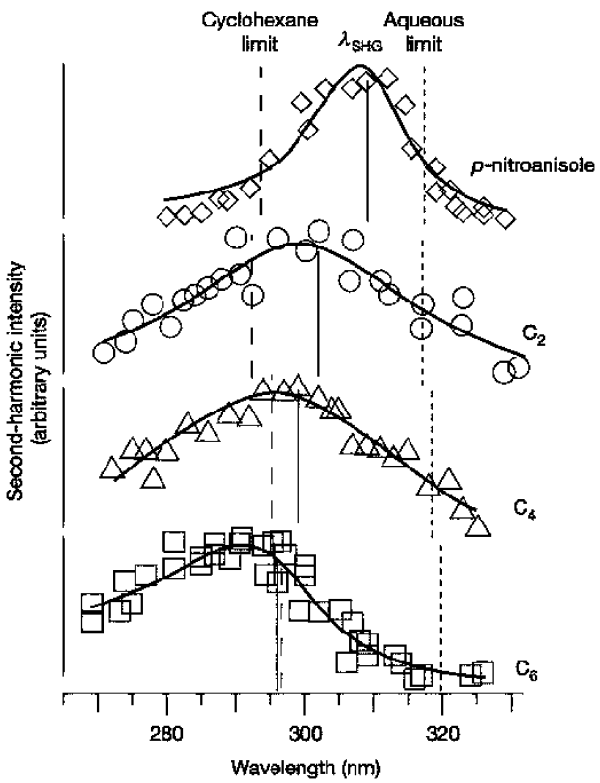

Fig. 4 Resonance-enhanced SHG spectra of (top to bottom) *p*-nitroanisole, C_2 rulers, C_4 rulers, and C_6 rulers adsorbed to a cyclohexane/water interface. Dashed and dotted lines denote excitation maxima in bulk cyclohexane and water, respectively. Solid vertical lines correspond to SHG maxima (λ_{SHG}) as determined by fitting the data. Note that SHG maxima do not always correspond to the wavelengths with highest SHG intensity, owing to the nonresonant contribution to $\chi^{(2)}$. Reprinted with permission from ref. 10. © Nature Publishing Group 2003.

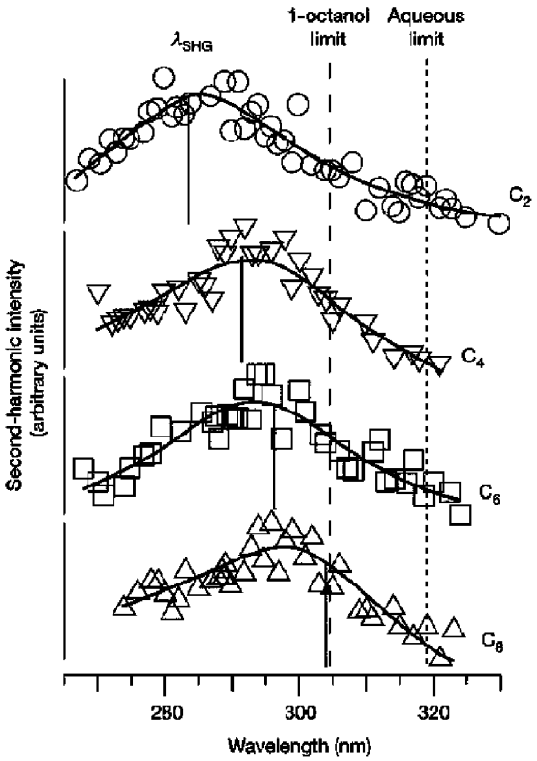

Fig. 5 Resonance-enhanced SHG spectra of (top to bottom) C_2 rulers, C_4 rulers, C_6 rulers, and C_8 rulers adsorbed to a 1-octanol/water interface. Dashed and dotted lines denote excitation maxima in bulk octanol and water, respectively. Solid vertical lines correspond to SHG maxima (λ_{SHG}) as determined by fitting the data. Reprinted with permission from ref. 10. © Nature Publishing Group 2003.

VSFS, two laser beams, one visible and one tunable infrared (IR), are overlapped on the interface, both in time and in space. These two beams then generate a third beam at the sum of the frequencies of the two incident beams. The intensity of the generated sum-frequency beam is given by

$$I(\omega_{SF}) \propto \left|\chi^{(2)}_{NR} + \sum_{v} \chi^{(2)}_{v}\right|^2 I(\omega_{vis}) I(\omega_{IR}) \tag{4}$$

where χ_{NR} and χ_{ν} are the nonresonant and resonant nonlinear susceptibility, respectively. $I(\omega_{vis})$ is the intensity of the visible beam, and $I(\omega_{IR})$ is the intensity of the infrared beam. Additionally, χ_{ν} can be written as

$$\chi^{(2)}_{v} \propto \frac{A_K M_{IJ}}{(\omega_v - \omega_{IR} - i\Gamma_v)} \tag{5}$$

where A_K is the IR transition moment, M_{IJ} is the Raman transition polarizability, ω_{ν} is the vibrational transition frequency, ω_{IR} is the frequency of the IR beam, and Γ_{ν} is the transition line width. Tuning the IR beam over a vibrational transition therefore results in an enhancement of the generated sum-frequency signal, giving a spectrum of the interfacial molecules. Therefore, VSFS can be used to study molecules that have vibrations that lie within the range of tunability of the IR source, making it applicable to a wider range of molecules. The polarizations of all three beams can be selected in order to obtain orientational information about the interfacial molecules. The most commonly employed polarization scheme is ssp, where the sum-frequency is s-polarized, the visible is s-polarized, and the infrared is p-polarized.

The first application of VSFS to the study of a liquid/liquid interface was by Richmond and coworkers, who used it to study the adsorption of sodium dodecyl sulfate (SDS) at the CCl_4/D_2O interface.[11] These initial measurements demonstrated that VSFS was a powerful tool that could be applied to obtain information about these buried interfaces. D_2O was used in these studies instead of H_2O to eliminate the overlap of the intensity of the O–H stretching modes with the C–H modes of interest. The success of this experiment was largely due to the use of a total internal reflection (TIR) geometry, which enhanced the weak signal to a detectable level.

Since VSFS is a nonlinear optical technique, the generated signal is weak, especially with nanosecond lasers, which have lower peak intensities relative to picosecond and femtosecond lasers. In addition to the resonant enhancement, the sum-frequency intensity is also dependent on the linear Fresnel factors for the input beams and the nonlinear Fresnel factor for the generated sum-frequency beam. In the TIR geometry, the visible beam is brought to the interface through the liquid with the higher index of refraction, and with the incident angle at or just past the critical angle such that it is totally internally reflected. By using this configuration, the sum-frequency signal is enhanced by several orders of magnitude.[12]

In addition to proving that VSFS is a viable technique for studying liquid/liquid interfaces, the work by Messmer *et al.* also provided evidence for the interfacial ordering of the adsorbed surfactant.[11,12] By using the ssp polarization scheme and comparing the relative intensities of the symmetric stretches of the methyl group on the end of the chain (2866 cm^{-1}) and the methylenes in the chain (2844 cm^{-1}), they were able to determine that the chain ordering increased as the interfacial surfactant concentration increased. The methyl symmetric stretch is largest for alkyl chains in an entirely *trans* configuration. As the number of *gauche* defects in the chains increases, the intensity of the methyl peak decreases, and the intensity of the methylene peak increases. The methylene intensity remained relatively constant as the concentration was increased, but the methyl intensity increased significantly, indicating that the chains were reorienting such that a larger number of chains were oriented with the dipole transition moments of the methyl groups having a component normal to the interfacial plane.

More recent surfactant studies at liquid/liquid interfaces detailed the adsorption of other surfactants at the CCl_4/D_2O interface[13] and at the d_{34}-hexadecane/D_2O interface.[14] The work by Watry and Richmond[13] examined the adsorption of linear alkylsulfonate and linear alkylbenzene sulfonate surfactants at the CCl_4/D_2O interface. These two classes of molecules make up a significant percentage of the surfactants used in the detergent industry, making it important to understand their properties at interfaces. It was found that the alkyl chains of dodecylbenzene-sulfonate are much more disordered at the interface than those of dodecanesulfonate. The increased degree of disorder is attributed to the presence of the benzene ring, which exists at the interface in a staggered arrangement.

Bain and coworkers have developed a new experimental arrangement to acquire VSFS spectra of hexadecyltrimethylammonium bromide (CTAB) at the hexadecane/water interface (Fig. 6).[14] By using a thin film of d_{34}-hexadecane and D_2O with the protonated surfactant, they were able to minimize the absorption of the infrared beam by the C–H stretches of the hexadecane. At low concentrations, it was found that CTAB forms conformationally disordered monolayers. As the concentration of the CTAB approached the critical micelle concentration (c.m.c.), the spectra show a change to a more ordered, upright chain conformation, as might be expected from the previous surfactant studies already discussed.

Another focus of VSFS studies of liquid/liquid interfaces has been on the interfacial structure and orientation of water at the water/organic liquid interface. The CCl_4/water interface provides an excellent starting point, since the CCl_4 is transparent in the C–H and O–H stretching regions, in contrast to many hydrophobic liquids. The VSFS spectrum of the neat CCl_4 interface is presented in Fig. 7, along with the individual peaks that were used to fit the spectrum.[15] The free OH feature arises from water molecules that straddle the interface, with one O–H pointing into the CCl_4 and the other pointing into the water, as depicted in Fig. 8. The O–H pointing into the CCl_4 cannot hydrogen bond, and is therefore at a higher energy than the other O–H bond, or donor OH, which is hydrogen-bonded to other water molecules. The frequency of the free OH band is slightly red-shifted from what is measured for the air/water interface. This demonstrates the presence of a weak CCl_4/H_2O interaction at this interface that results in the molecular orientation of the water molecules. Also observed are donor OH modes, tetrahedrally coordinated water molecules within

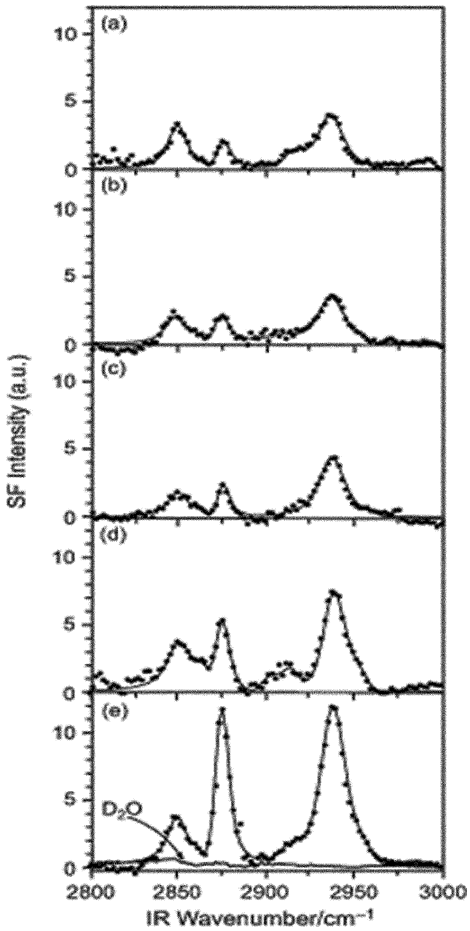

Fig. 6 SF spectra of CTAB at the oil/water interface (ssp-polarization). From top to bottom: (a) 0.05 mM CTAB, (b) 0.1 mM CTAB, (c) 0.3 mM CTAB, (d) 0.5 mM CTAB, (e) 0.6 mM CTAB compared with pure D_2O. Reprinted with permission from ref. 14. © American Chemical Society 2003.

the interfacial region, and the symmetric and antisymmetric stretching modes of monomeric water molecules.

The interfacial structure and orientation of alkane/water interfaces have also been studied, and subsequently compared with the CCl_4/water results.[16] Fig. 9 shows the VSFS spectra of three different alkane/water interfaces using the ssp polarization combination. The spectra of the interfaces of water with hexane, heptane and octane are all very similar to that of the CCl_4/water spectrum. However, the free OH is slightly blue-shifted from that of the CCl_4/water interface, indicating that the interaction between the water and the hexane, heptane and octane is slightly weaker. The free OH intensities are also lower than for the CCl_4/water interface, which is consistent with the weaker interaction between water and the alkanes. The weaker interaction could give the water molecules more rotational freedom, producing more possible orientations of the interfacial water molecules, and thus lower VSF intensities. To obtain a more complete picture of the interfacial water structure, Richmond and coworkers have complimented their VSFS studies with molecular dynamics simulations that allow the calculation of the number density of various interfacial water species.[16] This combination of theory and experiment allows the development of other interfacial molecular models while also providing information about isotropically oriented molecules that is difficult to obtain with VSFS.

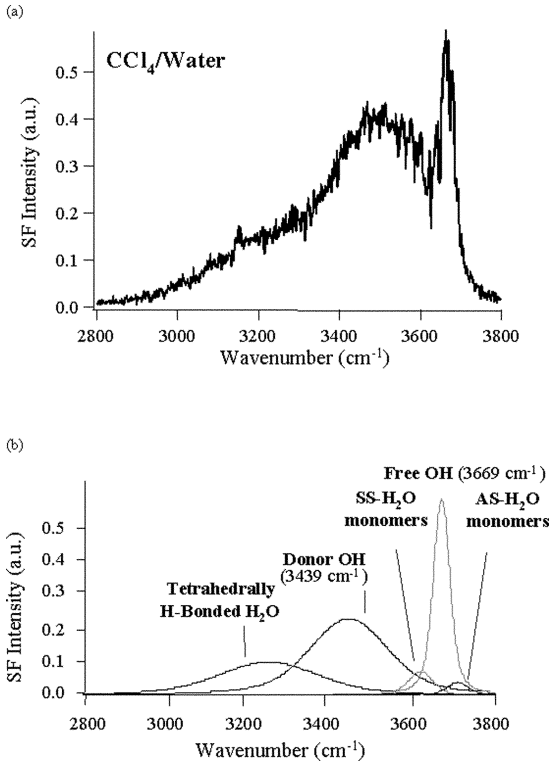

Fig. 7 (a) VSFS spectrum of the neat CCl_4/water interface (ssp polarization). (b) Individual peaks that contribute to the spectrum, derived from a nonlinear least squares fit to the data.

The 1,2-dichloroethane (DCE)/water interface has drawn considerable attention due to its electrochemical relevance as an interface between two immiscible electrolyte solutions.[6,17,18] Of particular issue is the question of whether the interfacial region consists of two separate and distinct phases or whether there is a significant degree of mixing between the two layers. To help further the understanding of this system, VSFS spectra were taken of the (CCl_4 + DCE)/water interface with varying mole fractions of DCE, from pure CCl_4 to pure DCE, and are presented in Fig. 10.[19] The loss of the free OH peak in the DCE/water spectrum and the overall decrease in the sum-frequency

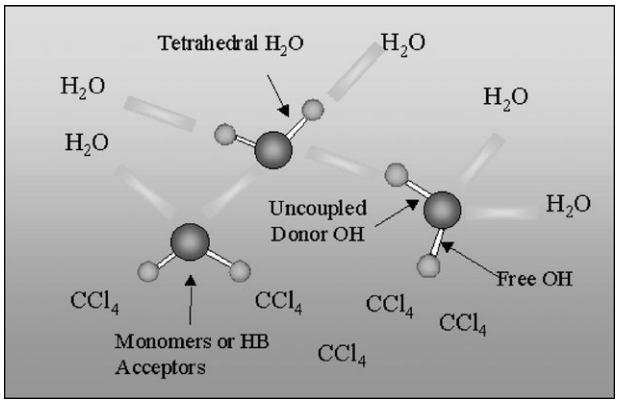

Fig. 8 Schematic of the interfacial water species contributing to the VSF spectrum of the neat CCl_4/water interface. Labeled species correspond to individual peaks from the spectra fit.

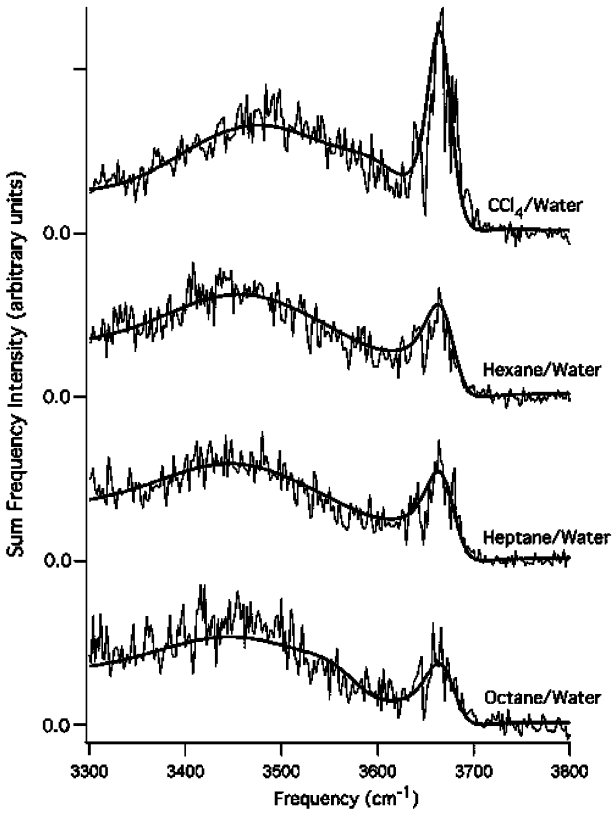

Fig. 9 VSF spectra of the CCl_4/water, hexane/water, heptane/water, and octane/water interfaces (ssp polarization). The solid lines are fits to the experimental data. Reprinted with permission from ref. 16. © American Chemical Society 2003.

intensity as the mole fraction of DCE increases indicate that the interfacial water molecules are more randomly oriented than at the CCl_4/water interface, and are hydrogen bonding with other water molecules.

The solvation of charge at a liquid/liquid interface has been the focus of a series of VSFS studies by Scatena and Richmond.[20] These studies examine the structure and bonding of water around the charged head group of isolated surfactants adsorbed to the CCl_4/water interface. As shown in Fig. 11, trace amounts of SDS have a dramatic effect on the interfacial water spectrum, making it possible to measure the solvation shell spectrum at very low surfactant concentrations. Water in the solvation shell is found to be highly oriented and displays weak hydrogen bonding interactions with adjacent water molecules in the interfacial region. As the concentration increases, the hydration shells begin to interact with each other, leading to the observed red-shifting of the water peak, which is indicative of stronger hydrogen bonding. By monolayer coverage, the hydrogen bonding has become even stronger, with the spectrum being dominated by signal from tetrahedrally coordinated water molecules.

Ellipsometry

Ellipsometry is another optical technique that can be applied to the study of liquid/liquid interfaces. By comparing the polarization states of the beam before and after it is reflected off of the interface, many optical material properties can be determined, such as the interfacial thickness and refractive index. As with many other properties, the surface refractive index is often different than that of the bulk for sensitive studies. Using the settings for the waveplates and polarizers in the ellipsometer,

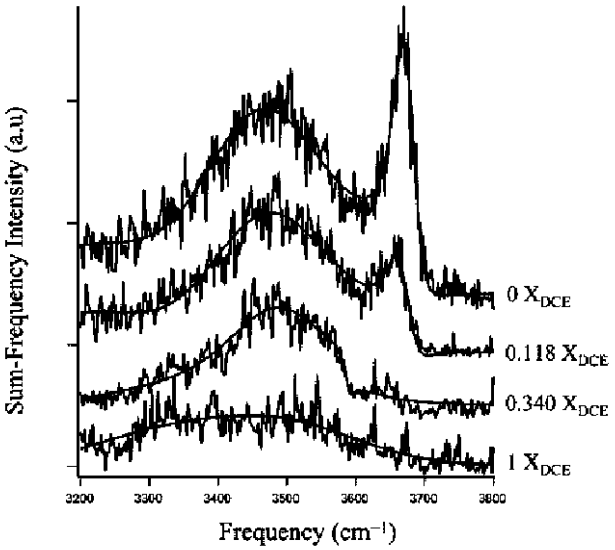

Fig. 10 VSF spectra of water at (DCE + CCl_4)/H_2O interfaces (ssp polarization). The top graph ($X_{DCE} = 0$) corresponds to the pure CCl_4/H_2O interface, and the bottom graph ($X_{DCE} = 1$) corresponds to the pure DCE/H_2O interface; the remaining graphs correspond to indicated mole fractions of DCE at the (DCE + CCl_4)/H_2O interface. Spectra are offset vertically for visual clarity. Reprinted with permission from ref. 19. © American Chemical Society 2004.

the ellipsometric parameters Ψ and Δ can be determined. These parameters, which characterize the polarization of the reflected light, can be used to calculate the complex ratio of the Fresnel coefficients.

$$\frac{r_p}{r_s} = \rho = \tan\psi e^{i\Delta} \tag{6}$$

where r_p is the reflection coefficient for p-polarized light and r_s is the reflection coefficient for s-polarized.

While surface freezing had been observed for long-chain alkanes at the air/alkane interface,[21] it had not been observed at the alkane/water interface. Recently, however, Lei and Bain have shown that the addition of a simple cationic surfactant can induce surface freezing at the tetradecane/water interface.[22] Using ellipsometry, they have shown that the presence of hexadecyltrimethylammonium bromide (CTAB) can induce surface freezing at the tetradecane/water interface. The coefficient of ellipticity, $\bar{\rho}$, was measured as a function of temperature (Fig. 12). $\bar{\rho}$ is defined as $\mathrm{Im}(r_p/r_s)$ at the Brewster angle θ_B, where θ_B is the angle where $\mathrm{Re}(r_p/r_s)$. The coefficient of ellipticity, which is related to the interfacial thickness, shows a large change indicative of a first order phase transition at 12 °C, which is 6 °C above the bulk melting point of tetradecane. The effect can be observed even for mole fractions of CTAB as low as 0.1. By modeling the ellipsometric data, it was determined that the frozen layer has a thickness of one monolayer, and the chains are densely packed and oriented nearly normal to the interface. This study is the first known observation of surfactant-induced surface freezing at an alkane/water interface.

Another recent study using ellipsometry to study liquid interfaces is that of Binks *et al.*, in which monodisperse silica particles (25 nm diameter) were studied at the toluene/water interface.[23] Ellipsometric studies were performed to determine the contact angles of the hydrophobized particles at the interface. However, the agreement between experiment and theory is not sufficient to calculate the contact angle. Although the results showed that ellipsometry alone is not sufficient for determining the contact angles in these systems, other interesting information was obtained. It was determined that the surface is not smooth, and is about three layers thick, as shown in Fig. 13. They also observed a large change in the ellipsometric parameter Δ, but little change in Ψ with

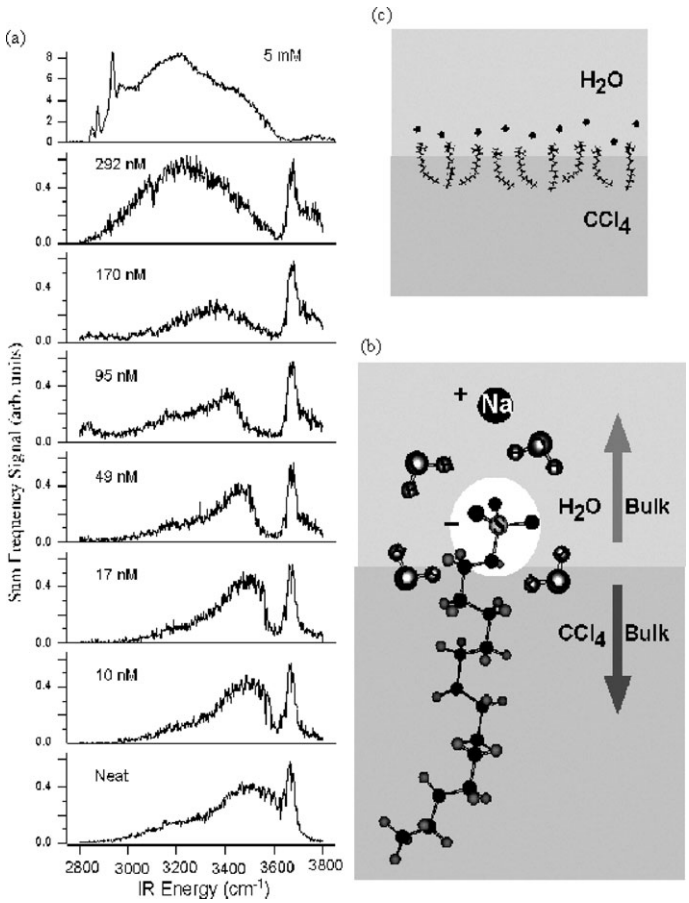

Fig. 11 (a) VSF spectra of the CCl_4/water interface with increasing concentrations of SDS, from the neat interface to 5 mM SDS (monolayer coverage) (ssp polarization). (b) Schematic of an SDS molecule adsorbed to the interface, along with the water molecules solvating the head group. (c) Schematic of a monolayer of SDS molecules ordering at the CCl_4/water interface.

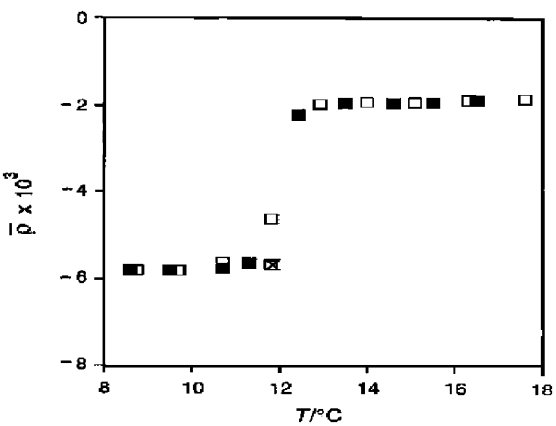

Fig. 12 Coefficient of ellipticity $\bar{\rho}$ as a function of temperature for the interface between a 0.6 mM solution of CTAB and tetradecane. Reprinted with permission from ref. 22. © American Physical Society 2004.

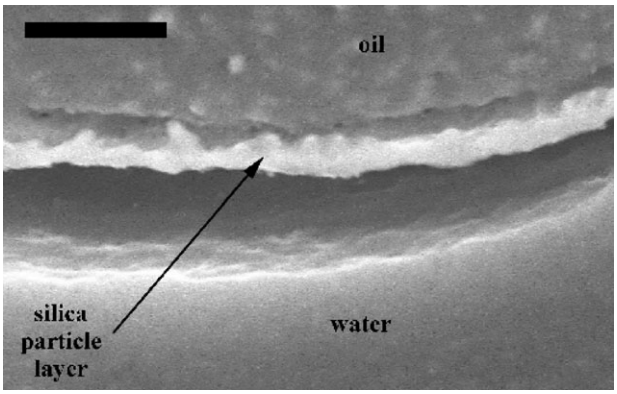

Fig. 13 Freeze–fracture SEM image of an oil-in-water emulsion drop stabilized with 25 nm diameter hydrophobized silica particles, showing a section through the oil/water interface. The bar is 500 nm. Reprinted with permission from ref. 23. © American Chemical Society 2003.

increasing amounts of particles spread at the interface, which can be seen in Fig. 14. At low concentrations up to monolayer coverage, theoretical calculations of Δ agree well with experimental results. At high concentrations, the results are consistent with a surface coverage greater than a close-packed monolayer or a corrugated monolayer with an amplitude smaller than the particle radius.

Brewster angle microscopy

Brewster angle microscopy (BAM) has been used for a number of years to study air/liquid interfaces, but has only recently been applied to liquid/liquid interfaces.[24] BAM is a space-resolved imaging ellipsometric technique in which a beam is brought to the neat interface at Brewster's angle. The subsequent adsorption of surfactants to the interface then changes the interfacial refractive

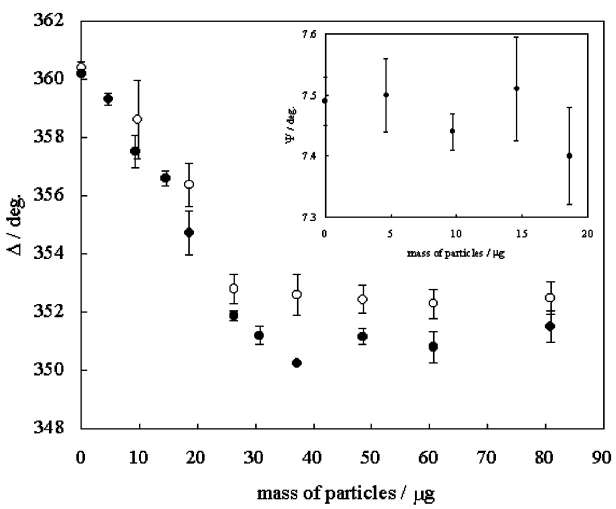

Fig. 14 Ellipsometric parameter Δ for hydrophobized silica particles, with a diameter of 25 nm, at the toluene/water interface, plotted against the mass of particles spread. ○, particles spread from methanol; ●, particles spread from 2-propanol. The inset shows the ellipsometric parameter Ψ plotted against the mass of the particles. Reprinted with permission from ref. 23. © American Chemical Society 2003.

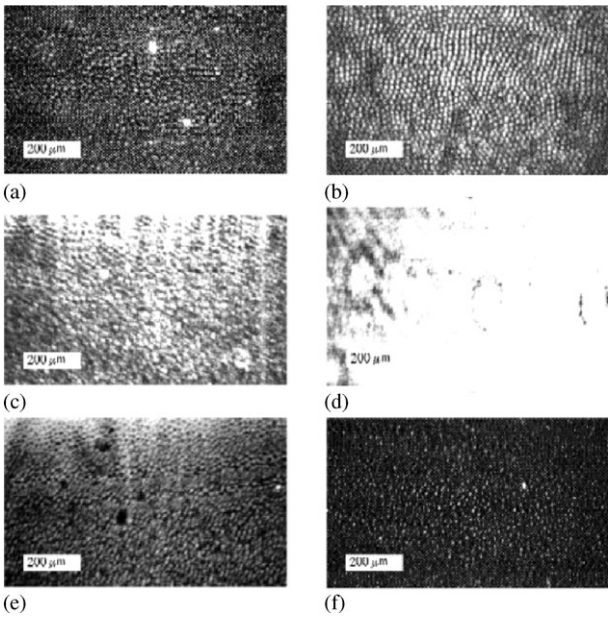

Fig. 15 BAM images of an adsorbed film of $FC_{12}OH$ at the hexane/water interface at different temperatures: (a) 21 °C, (b) 20 °C, (c) 15 °C, (d) 12 °C, (e) 15 °C, (f) 23 °C; (a–d) stepwise decrease of T; (e, f) stepwise increase of T. Reprinted with permission from ref. 24. © American Chemical Society 1999.

index and therefore the magnitude of the reflected portion of the beam, allowing the imaging of domain patterns of adsorbates.

The first application of BAM to the study of liquid/liquid interfaces was by Uredat *et al.*, in which BAM was used to study temperature-induced phase transitions in Gibbs monolayers of octadecanol ($C_{18}OH$) and 1,1,2,2-tetrahydroperfluorododecanol ($FC_{12}OH$) at the hexane/water interface.[24] The BAM images of $FC_{12}OH$ are shown in Fig. 15. At 21 °C, small domains of the condensed film are visible at the interface. As the temperature is decreased, the size and interfacial coverage of these domains increase. At the lowest temperature, 12 °C, the condensed phase seems to have entirely covered the interface. The final two frames of Fig. 15 show the films as the temperature is increased. Increasing the temperature from 12 °C to 15 °C produces dark patches in the films, which are attributed to ''holes'' in the film caused by a gas-like film within the condensed phase, even though the temperature is still well below the phase transition temperature ($T_t = 24 \pm 1$ °C). Finally, when the temperature is increased to the phase transition temperature, small domains of the condensed phase can be seen in coexistence with the gas-like phase.

Fig. 16 presents BAM images showing the domain patterning of $C_{18}OH$ at the hexane/water interface at 15 °C, 12 °C and 10 °C. The condensed phase domains are generally larger for $C_{18}OH$ than for $FC_{12}OH$. All of these temperatures are below the phase transition temperature of 24 °C. At 15 °C and 12 °C, the images are dominated by regions that are roughly circular, but at 12 °C these circular regions coexist with continuous regions of the condensed phase, as seen in Fig. 16b. When the temperature is decreased to 10 °C, the image shows bands of the continuous regions and oval, deformed domain regions oriented along the direction of flow within the interface. When the temperature is held constant and the system is monitored over time (Fig. 16d–f), the domains become polyhedral in shape and eventually are composed almost entirely of the continuous, condensed phase. The final image shows the crystallization of the interface after 111 min. Surprisingly, the coexistence of the condensed and expanded phases of the $C_{18}OH$ is not limited to a single temperature, as is expected for a first-order phase transition, but instead extends over $\sim$15 K below the phase transition temperature. This behavior can be attributed to trace surface-active impurities.

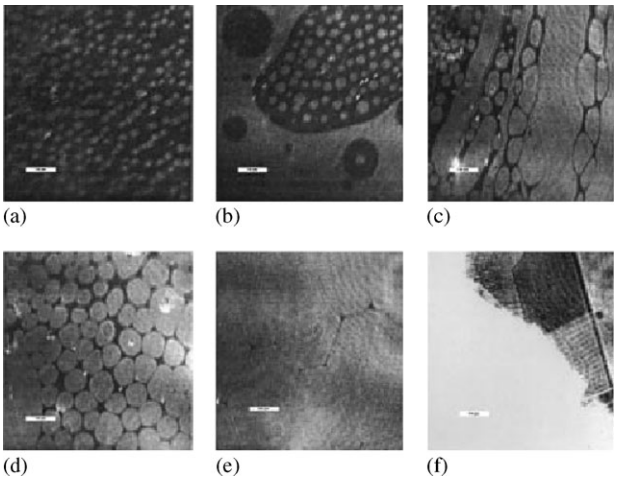

Fig. 16 BAM images of $C_{18}OH$ at the hexane/water interface, showing domain structures along a descending scan below the phase transition temperature (T_t = 24 °C): (a) 15 °C, (b) 12 °C, (c–f) 10 °C, and illustrating the evolution of domain patterns as a function of time after the temperature step from 12 to 10 °C for (c) 45 min, (d) 100 min, (e) 108 min, and (f) 111 min. The white bar represents a length of 100 μm. Reprinted with permission from ref. 24. © American Chemical Society 1999.

Total internal reflection fluorescence spectroscopy (TIRFS)

Through the use of a fluorescent dye as a probe, total internal reflection fluorescence spectroscopy (TIRFS) provides a method for studying adsorption at liquid/liquid interfaces. In TIRFS, a laser beam is directed onto a liquid/liquid interface in a total internal reflection geometry. The incident beam is polarized perpendicular to the incident plane (s-polarized), and the incident angle is chosen to be sufficiently greater than the critical angle for total internal reflection. When the beam hits the interface in a TIR geometry, it induces an evanescent wave that decays exponentially with vertical distance from the interface, allowing molecules at or near the interface to be probed. Since fluorescence is not inherently surface-specific, signals can arise from molecules in the bulk liquid. To remove any unwanted bulk signal, the fluorescence is measured both from the interface and from the bulk incident medium to allow subtraction of the background fluorescence signal.[25]

In a recent study, Yamashita *et al.* used TIRFS to study the solvation dynamics of two fluorophores (Fig. 17) at the heptane/water interface.[26] The fluorophores, 12-(9-anthroyloxy) stearic acid (12-AS) and 4-(9-anthroyloxy) butanoic acid (4-ABA), both have an anthroyloxy group as their fluorophore, and the emission wavelength is known to be a good indicator of the polarity of the solvent. Both probe molecules have emission wavelengths of ~480 nm in methanol and ~460 nm in heptane, which shows that the emission wavelength depends on the fluorophore

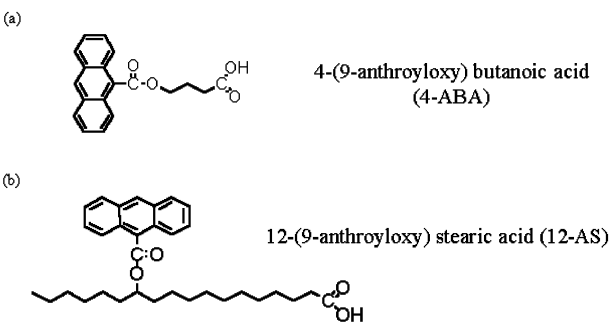

Fig. 17 Structures of (a) 4-(9-anthroyloxy) butanoic acid (4-ABA) and (b) 12-(9-anthroyloxy) stearic acid (12-AS).

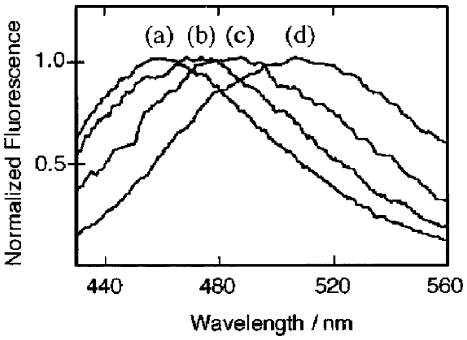

Fig. 18 Fluorescence spectra of 12-AS and 4-ABA. (a) 1×10^{-5} M 12-AS in heptane. (b) 12-AS at the heptane/water interface. [12-AS] = 1×10^{-8} M in heptane. (c) 4-ABA at the heptane/water interface, [4-ABA] = 5×10^{-6} M in phosphate buffer (pH 7.0). (d) 1×10^{-5} M 4-ABA in aqueous phosphate buffer (pH 7.0). Reprinted with permission from ref. 26. © American Chemical Society 2003.

and not on the structure of the rest of the molecule, making comparisons possible between the different molecules in their respective solvent layers.

The oil-soluble fluorophore, 12-AS, was studied in heptane and at the heptane/water interface, and the water-soluble fluorophore, 4-ABA, was studied in a pH 7 phosphate buffer and at the heptane/phosphate buffer interface. As evidenced by Fig. 18, the emission maximum of each fluorophore shifts between the bulk solvent and the heptane/aqueous interface, showing that the polarity of the heptane/water interface is between the polarities of bulk heptane and water. Further, the fluorescence maxima for 4-ABA and 12-AS at the heptane/water interface differ from each other, with 4-ABA red-shifted relative to 12-AS. This indicates that the probe molecules are in interfacial environments with different polarities, and that the solvation environment of the fluorophores at the heptane/water interface is dependent on the structure of the probe molecule.

The time-dependent fluorescence spectra of the two fluorophores at their respective interfaces and in a binary mixture of 3 M ethanol in heptane were also measured.[26] At the heptane/water interface, the emission wavelength of 12-AS showed a time-dependent red-shift, while the center wavelength of 4-ABA at the heptane/buffer interface remained unchanged. When the two fluorophores were studied in the mixture of ethanol and heptane, they both showed a time-dependent spectral shift. The results of these studies indicate that 12-AS undergoes preferential solvation at the heptane/water interface, with the fluorophore solvated by more heptane than water in the ground state and by more water than heptane in the excited state. On the other hand, 4-ABA does not undergo preferential solvation. It is solvated by more water molecules than heptane molecules, and is located closer to the water phase than 12-AS.

Another application of TIRFS to the study of liquid/liquid interfaces has been in the area of molecular recognition. Molecular recognition is important in biological systems, where it proceeds at microscopic interfaces such as cell and protein surfaces in the aqueous phase. It occurs through noncovalent interactions such as hydrogen bonding or electrostatic or hydrophobic interactions. However, due to experimental difficulties, only a few spectroscopic studies have been done at liquid/liquid interfaces.[27–29]

Recently, time-resolved TIRFS was used to observe molecular recognition mediated by hydrogen bonding at a CCl_4/water interface.[30] Riboflavin was placed in the aqueous phase, and was studied at the CCl_4/water interface with and without *N,N*-dioctadecyl-[1,3,5]triazine-2,4,6-triamine (DTT) in the CCl_4 phase (Fig. 19). These molecules are capable of forming triple hydrogen bonds with each other, but since they are soluble in different phases, it was expected that such a process should only occur at the interface. The fluorescence decay profiles of riboflavin in the absence of DTT were fit with a single-exponential, while a double-exponential was necessary to fit the decay measured in the presence of DTT. Fluorescence anisotropy was also used to measure reorientation times, which showed that both riboflavin and DTT have faster reorientation times than the hydrogen-bonded complex, thereby indicating that molecular recognition mediated by the formation of a triple hydrogen bonded complex can take place at an interface.

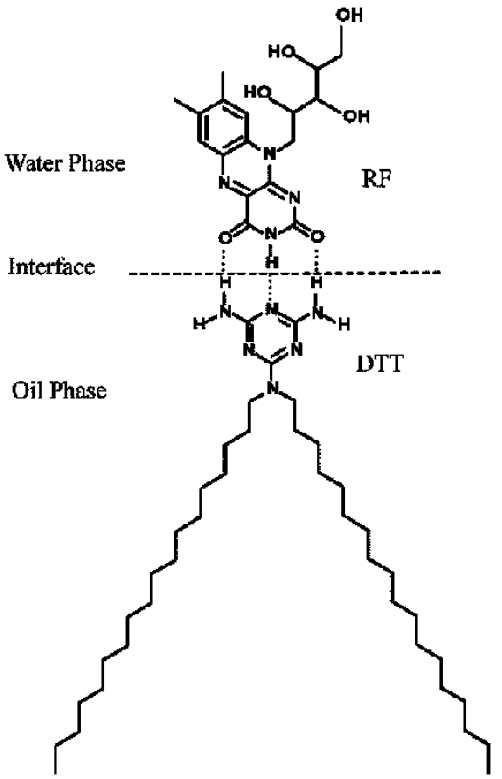

Fig. 19 Schematic of molecular recognition between riboflavin and DTT mediated by hydrogen-bonding interactions at an oil/water interface. Reprinted with permission from ref. 30. © American Chemical Society 2003.

X-Ray and neutron scattering

X-Ray and neutron scattering are increasingly being used to explore the liquid/liquid interface. Both scattering techniques are used to obtain information about the structure of thin films. This information is extracted by modeling the interface as a series of layers with different parameters that are adjusted until the model agrees with experimental results. Fig. 20 presents a vapor-tight stainless steel sample cell used for X-ray scattering measurements, which enables the study of the interface between two thin liquid layers in a vacuum environment.[31]

Li *et al.* used off-specular diffuse X-ray scattering to study monolayers of $CF_{12}OH$ at the hexane/water interface.[32] The system was studied previously with Brewster angle microscopy,[24] and has also been presented here. However, the use of X-ray scattering allowed access to domains that were smaller than the resolution of BAM. In this study, the size and distribution of the interfacial domains in $CF_{12}OH$ monolayers were probed as a function of temperature. It was found that the domain size and the mean separation distance remain constant over a range of temperatures, as can be seen in Fig. 21. In contrast, the interfacial coverage changes by a factor of ten over the same temperature range (Fig. 22). These results indicate that new domains are created or destroyed as the temperature is changed. Additionally, the domain sizes remain constant when heating and cooling through the solid–gas transition. This suggests that the domain sizes are at equilibrium, which can be established through the exchange of $CF_{12}OH$ molecules between the monolayer and the bulk hexane solution.

Another recent study of a liquid/liquid interface uses X-ray reflectivity to study the interface between water and *n*-alkanes with carbon numbers 6–10, 12, 16, and 22.[31] Fig. 23 presents the logarithm of the X-ray reflectivity, normalized to the Fresnel reflectivity, for each of the interfaces

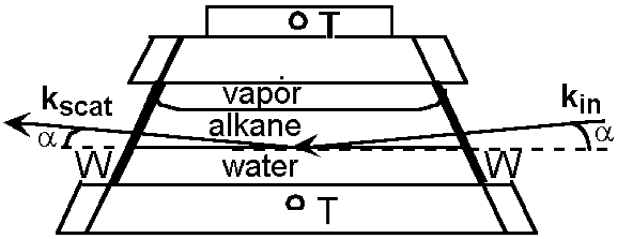

Fig. 20 Cross-sectional view of sample cell: W, Mylar windows; T, thermistors to measure temperature. The kinematics of surface X-ray reflectivity is also indicated: $\boldsymbol{k}_{in}$ is the incoming X-ray wave vector, $\boldsymbol{k}_{scat}$ is the scattered wave vector, and α is the angle of incidence and reflection. Reprinted with permission from ref. 31. © American Physical Society 2000.

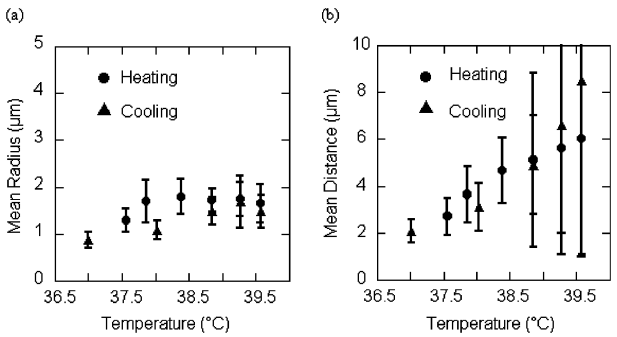

Fig. 21 (a) Mean radius of domains ($\bar{R}$) *vs.* temperature and (b) mean separation distance between domains ($\bar{D}$) *vs.* temperature. ●: heating curve; ▲: cooling curve. The error bars indicate $\pm\sigma_{R,D}$, a measure of polydispersity in $\bar{R}$ and $\bar{D}$. Reprinted with permission from ref. 32. © EDP Sciences 2002.

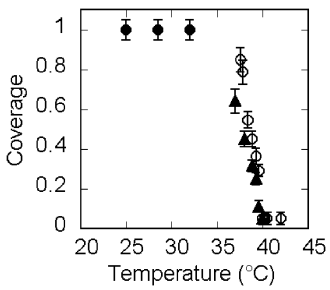

Fig. 22 Interfacial coverage (fraction of interface covered by the low-temperature solid phase) as a function of temperature. ○: heating curve; ▲: cooling curve; ●: from earlier reflectivity measurements. Reprinted with permission from ref. 32. © EDP Sciences 2002.

studied. The solid lines are one parameter fits to the reflectivity $R(Q_z)$

$$R(Q_z) = R_F(Q_z)e^{-Q_z Q_z^T \sigma^2} \cong \left|\frac{Q_z - Q_z^T}{Q_z + Q_z^T}\right|^2 e^{-Q_z Q_z^T \sigma^2} \quad (7)$$

where $R_F(Q_z)$ is the Fresnel reflectivity calculated for an ideal, zero width, step-like interface, Q_z is the wave vector transfer in the z direction, given by $Q_z = (4\pi/\lambda)\sin\alpha$, $Q_z{}^T$ is the z component of the

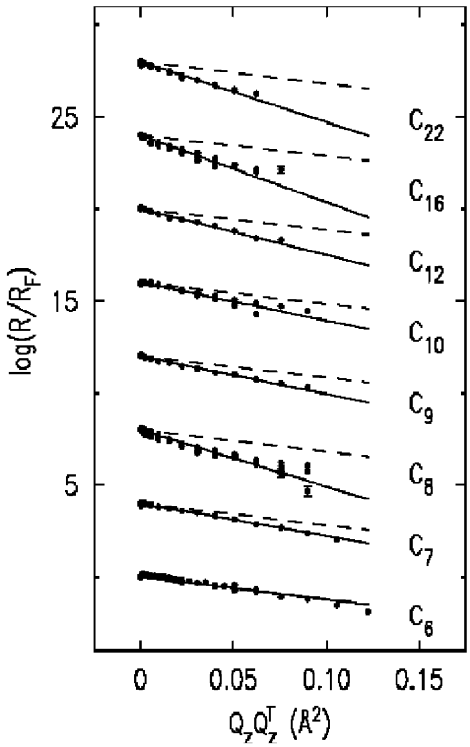

Fig. 23 Logarithm of X-ray reflectivity, normalized to Fresnel reflectivity $R_F(Q_z)$, as a function of $Q_zQ_z^T$, for water/alkane interfaces for eight different *n*-alkanes. Curves for the different interfaces are offset for clarity. The solid lines are one parameter fits of the measurements. The slopes of the fits are the interfacial width, σ. Also shown with dashed lines are predicted reflectivity curves for interfaces whose width is determined solely by capillary waves. Reprinted with permission from ref. 31. © American Physical Society 2000.

wave vector transfer with respect to the lower phase, and the fitting parameter σ represents the interfacial width. The dashed lines are the predicted reflectivity curves using only capillary-wave theory to predict the interfacial width. The measured interfacial width of the hexane/water interface agrees well with the prediction of capillary-wave theory. However, capillary-wave theory alone is not sufficient for predicting the interfacial width for the interfaces between water and the longer *n*-alkanes. Instead, these interfaces can be better described by a combination of capillary-wave theory and an intrinsic structural contribution. For short molecules, the gyration radius sets the length scale of the intrinsic interfacial structure, while the bulk correlation length sets the length scale for longer molecules.

A recent study by Bowers *et al.* has demonstrated how neutrons can be used to examine liquid/liquid interfaces.[33] This study involves interfaces of non-volatile oils and oil-soluble species. They have employed a spin–freeze–thaw technique to form an oil/water interface that is thin enough to transmit the neutron beam. The only assumption in this protocol is that the oil film is greater than 2000 Å, allowing the use of the thick film reflectivity formula. By using this new procedure, they were able to study the hexadecane/water interface, both neat and with the addition of polybutadiene (PB)–poly(ethylene oxide) (PEO) block copolymer. The neat hexadecane/water interface was found to be rougher than predicted by capillary-wave theory. Upon the addition of the PB–PEO copolymer, it was found that the copolymer segregates at the interface, as shown in Fig. 24. The blocks occupy a relatively thin, concentrated region immediately on either side of the interface that is about 20 Å thick and composed of about 20% polymer, followed, on each side, by a thicker, more dilute region which is about 50 Å thick and composed of less than 10% polymer.

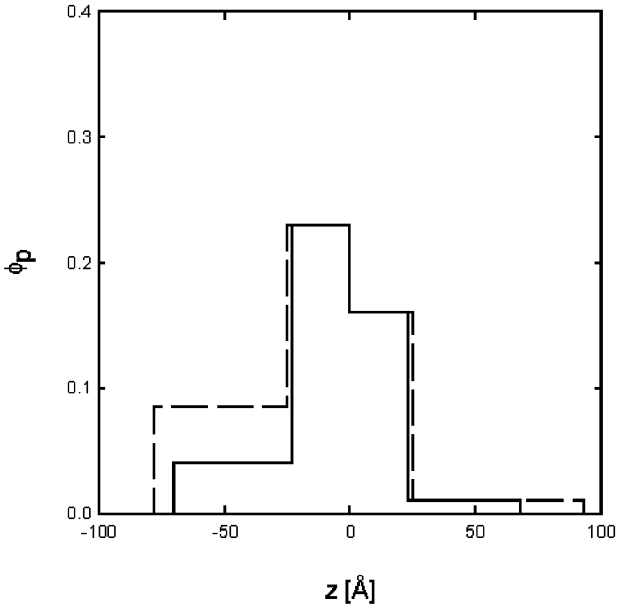

Fig. 24 Volume fraction profiles ϕ_p of the polymer distributions from modeled spectra. The dividing surface $z = 0$ is placed at the position of PB/PEO block segregation. Interfacial concentration $\Gamma = 4$ mg m^{-2} (–); $\Gamma =$ 10 mg m^{-2} (--). Reprinted with permission from ref. 33. © American Chemical Society 2001.

Future directions

The molecular properties of liquid/liquid interfaces have long been a subject of interest. There is a clear need for an expanded understanding of the molecular structure and bonding at liquid/liquid interfaces because these properties determine the interfacial kinetic and thermodynamic processes. Only recently, however, has molecular level information about these systems been obtainable. A few recent studies have been presented here, highlighting several emerging experimental methods, as well as providing some examples of current systems of interest. The future of this research is promising, with many exciting areas to be explored.

Determination of the widths of these interfaces continues to be an area of interest, and is being studied with a number of techniques. Characterizing different interfaces as molecularly sharp or as a more diffuse, mixed interfacial region is important for a better understanding of those interfaces. Many of the studies that have been done on liquid/liquid interfaces have focused on the equilibrium properties. However, the dynamics that occur at interfaces are equally important to our understanding of interfacial processes. Recent advances in short pulse-width lasers have enabled the study of interfacial dynamics, such as reactions and adsorption processes.

Molecular adsorption to liquid/liquid interfaces is another area that has many exciting opportunities. Ongoing studies of surfactants and biologically relevant molecules at interfaces are focusing on the effect of the adsorbed molecules on the structure and orientation of the interfacial water molecules, and their interaction with the adsorbates. Also of interest is the interaction of the adsorbates with each other. Studies are focusing on understanding the environment of isolated adsorbates, as well as the overall interfacial structure in the presence of large numbers of adsorbed molecules and whether they form an even distribution or islands at the interface. Other studies are focusing on the effect of electrolytes on the structure and orientation of interfacial water molecules. The potentials across liquid/liquid interfaces provide yet another area for study, and modeling these interfacial potentials will further our understanding of these systems. Molecular transport across interfaces is also of great relevance, especially to biological applications, and it is important to continue to improve our understanding of the barriers to the transport across the liquid/liquid interface on a molecular level. Although this review has not addressed theoretical advances in

modeling and understanding these interfaces, the coupling of theory and experiment to the study of liquid/liquid interfaces will be invaluable for further advances in the field.

Acknowledgements

The authors thank Cathryn McFearin and Adam Hopkins for their help with this review, and the National Science Foundation (CHE-0243856), the Department of Energy, Basic Energy Sciences (DE-FG-03-96ER45557), and the Office of Naval Research for funding. Prof. Richmond is very appreciative for being honored with the Spiers Lecture Award.

References

1 Y. R. Shen, *Annu. Rev. Phys. Chem.*, 1989, **40**, 327.
2 K. B. Eisenthal, *Chem. Rev.*, 1996, **96**, 1343.
3 J. C. Conboy, J. L. Daschbach and G. L. Richmond, *J. Phys. Chem.*, 1994, **98**, 9688.
4 R. M. Corn and D. A. Higgins, *Chem. Rev.*, 1994, **94**, 107.
5 S. G. Grubb, M. W. Kim, T. Rasing and Y. R. Shen, *Langmuir*, 1988, **4**, 452.
6 J. C. Conboy and G. L. Richmond, *Electrochim. Acta*, 1995, **40**, 2881.
7 T. Uchida, A. Yamaguchi, T. Ina and N. Teramae, *J. Phys. Chem. B*, 2000, **104**, 12091.
8 Y. R. Shen, *The Principles of Nonlinear Optics*, Wiley, New York, 1984.
9 H. Wang, E. Borguet and K. B. Eisenthal, *J. Phys. Chem. B*, 1998, **102**, 4927.
10 W. H. Steel and R. A. Walker, *Nature*, 2003, **424**, 296.
11 M. C. Messmer, J. C. Conboy and G. L. Richmond, *J. Am. Chem. Soc.*, 1995, **117**, 8039.
12 J. C. Conboy, M. C. Messmer and G. L. Richmond, *J. Phys. Chem.*, 1996, **100**, 7617.
13 M. R. Watry and G. L. Richmond, *J. Am. Chem. Soc.*, 2000, **122**, 875.
14 M. M. Knock, G. R. Bell, E. K. Hill, H. J. Turner and C. D. Bain, *J. Phys. Chem. B*, 2003, **107**, 10801.
15 L. F. Scatena, M. G. Brown and G. L. Richmond, *Science*, 2001, **292**, 908.
16 M. G. Brown, D. S. Walker, E. A. Raymond and G. L. Richmond, *J. Phys. Chem. B*, 2003, **107**, 237.
17 H. Jensen, D. J. Fermin and H. H. Girault, *Phys. Chem. Chem. Phys.*, 2001, **3**, 2503.
18 Z. Samec, *Chem. Rev.*, 1988, **88**, 617.
19 D. S. Walker, M. G. Brown, C. L. McFearin and G. L. Richmond, *J. Phys. Chem. B*, 2004, **108**, 2111.
20 L. F. Scatena and G. L. Richmond, *J. Phys. Chem. B*, 2004, **108**, 12518.
21 B. M. Ocko, X. Z. Wu, E. B. Sirota, S. K. Sinha, O. Gang and M. Deutsch, *Phys. Rev. E*, 1997, **55**, 3164.
22 Q. Lei and C. D. Bain, *Phys. Rev. Lett.*, 2004, **92**, 176103.
23 B. P. Binks, J. H. Clint, A. K. F. Dyab, P. D. I. Fletcher, M. Kirkland and C. P. Whitby, *Langmuir*, 2003, **19**, 8888.
24 S. Uredat and G. H. Findenegg, *Langmuir*, 1999, **15**, 1108.
25 S. Ishizaka, H.-B. Kim and N. Kitamura, *Anal. Chem.*, 2001, **73**, 2421.
26 T. Yamashita, T. Uchida, T. Fukushima and N. Teramae, *J. Phys. Chem. B*, 2003, **107**, 4786.
27 M. J. Crawford, J. G. Frey, T. J. VanderNoot and Y. Zhao, *J. Chem. Soc., Faraday Trans.*, 1996, **92**, 1369.
28 T. Kakiuchi, K. Ono, Y. Takasu, J. Bourson and B. Valeur, *Anal. Chem.*, 1998, **70**, 4152.
29 K. Nochi, A. Yamaguchi, T. Hayashita, T. Uchida and N. Teramae, *J. Phys. Chem. B*, 2002, **106**, 9906.
30 S. Ishizaka, S. Kinoshita, Y. Nishijima and N. Kitamura, *Anal. Chem.*, 2003, **75**, 6035.
31 D. M. Mitrinović, A. M. Tikhonov, M. Li, Z. Huang and M. L. Schlossman, *Phys. Rev. Lett.*, 2000, **85**, 582.
32 M. Li, A. M. Tikhonov and M. L. Schlossman, *Europhys. Lett.*, 2002, **58**, 80.
33 J. Bowers, A. Zarbakhsh, J. R. P. Webster, L. R. Hutchings and R. W. Richards, *Langmuir*, 2001, **17**, 140.